

CAAP Quarterly Report

09/30/2023

Project Name: Easy Deployed Distributed Acoustic Sensing System for Remotely Assessing Potential and Existing Risks to Pipeline Integrity

Contract Number: 693JK3215002CAAP

Prime University: Colorado School of Mines

Prepared By: Yilin Fan, yilinfan@mines.edu, 303-273-3749;
Ge Jin, gjin@mines.edu, 303-273-3455;
Ali Tura, alitura@mines.edu, 303-273-3454;
Jennifer Miskimins, jmiskimi@mines.edu, 303-384-2607

Reporting Period: [07/01/2023 – 09/30/2023]

Project Activities for Reporting Period:

During the past period, we have made noticeable progress, especially for Tasks#2 and #6. The following sections discuss the project activities for each remaining task, respectively. All the plots are attached in the appendix at the end of this document due to the page limitation.

Task#2. Detection of Dynamic Intermittent (Slug) Structure

In this task, we focused on detecting dynamic intermittent (slug) structures, and several significant activities were undertaken:

- Two pressure sensors were carefully positioned, one at the inlet's start downhill and another toward the outlet of the flow loop, uphill. These sensors were integrated into the LabView Data Acquisition system to facilitate precise data collection.
- To minimize vibration and noise associated with slug discharge into the tank, the outlet for the multiphase flow loop was revamped. The straight 1.5-in. pipes were replaced with a 45-degree inclined 4-in. PVC pipes. Figure 1 shows the picture of the revamped multiphase facility.
- Two new water pumps were connected to the flow loop, one for supply and the other for drainage, to replace the previous one that failed.
- A pressure relief valve was added to the water supply line for safety considerations.
- Figure 2 illustrates the experimental setup for Task#2, highlighting the placement of pressure sensors. Notably, flow direction in the DAS data alternated among the five different cables due to splicing at opposing ends.
- A series of experiments were conducted under controlled conditions. These included maintaining a constant water flow rate of 0.6 GPM (equivalent to 0.005 m/s) and systematically varying air velocities from 18 m/s to 2 m/s, the same as in the original proposal.
- Data collection encompassed both single-phase (air) and multi-phase (air and water) experiments, at the same air velocities.

- Field observations revealed distinct flow behaviors. Stratified flow was observed within velocities ranging from 18 m/s to 8 m/s, while intermittent slugging occurred at velocities ranging from 6 m/s to 2 m/s. Different cables effectively captured this slugging behavior, as evident in Figure 3.
- Processed DAS data allowed for the precise identification of slugs, which was correlated with data from pressure and flow meter sensors. Figure 4 demonstrates a good correlation, with high values corresponding to slug presence.
- The sensitivity of various cable types was evaluated by comparing a single channel near each pressure sensor for each cable type. Figure 5 reveals that flat cables exhibited the highest sensitivity, followed by thin, straight, helical, and thick cables.

Task#3. Detection of Corroded Spots on Pipeline Interior Surface

In this task, our primary focus, in line with the results reported in the previous quarterly report, was directed towards increasing the depth of corrosion within the 1-m section. Our efforts were initially centered on the creation of a new corroded 1-m section with a target depth of approximately 5.8 mm while keeping in mind that the pipe wall thickness stands at 6.019 mm. As illustrated in Figure 6, the corrosion induced by the hydrochloric acid penetrated the pipe wall at the bottom of the pipe (6 O'clock position), resulting in a minor leakage spot measuring approximately 2 mm in diameter. These outcomes are consistent with our earlier reported hypotheses and results for several reasons:

- The corrosion rate we previously calculated aligns closely with the findings observed during this conducted experiment.
- Our corrosion model has suggested the presence of irregularities on the interior surface, which are caused by the intentional scratches introduced during the experimental setup. These irregularities enabled the hydraulic acid to break through the pipe wall surface, resulting in the formation of the leakage spot.

The pipe in question is now ready to be tested in the flow loop once it is connected and will serve as a simulation of a severe corrosion scenario with a minor leakage. Meantime, we are developing another 1-m test section, with the objective of achieving a slightly shallower corroded depth of around 5.5 mm with no leakage. This adjustment accounts for measurement uncertainties and aims to mitigate the risk of another breakthrough occurrence. The aforementioned pipes will all undergo testing in the forthcoming reporting period.

Task#4. Detection of Dent/Deformation on Pipeline

During this reporting period, we worked with EMI (the Excavation Engineering and Earth Mechanics Institute) at the Colorado School of Mines on the fabrication of dents in the 1-m test section. We have successfully prepared two deformed pipes with different dent sizes. The pipe that exhibits a substantial deformation represents a significant structural compromise, while the other that showcases a smaller dent simulates a less severe scenario, as depicted in Figure 7. Our intention is to test these two differently deformed pipes in the flow loop during the upcoming reporting period.

Task#6. Detection of Leakage

During the past period, we repeated the leakage tests using a 1-m test section with 1-in. holes at three different positions to simulate the leakage at different orientations. With reducers, we were able to test four leakage sizes, namely $\frac{1}{4}$ ", $\frac{1}{2}$ ", $\frac{3}{4}$ ", and 1". A picture of the facility is shown in Figure 8. Five gas flow rates, 2, 6, 10, 14, 18 m/s, were tested. We also did the experiments at the same flow rates but without any leakage, which is referred to as the control tests thereafter.

During this task, the DAS data were recorded at a frequency of approximately 5600 Hz along a 480-meter fiber, generating a substantial volume of data in a short period. For instance, the three-hour recording session yielded over 150 GB of DAS data. Due to its size, this data set requires pre-processing before any meaningful analysis can be conducted. The first processing we conducted was based on the standard deviation (STD). We segment the data set into one-second intervals and compute the STD for each channel within each second. These STD values are then concatenated into a continuous data set with a 1 Hz sampling rate. This method allows for a data reduction factor of 5600, equivalent to the original sampling rate. Figure 9 provides an illustrative example of the STD data attributes during an experiment involving bottom leakage holes. In this figure, a higher value (depicted in red) signifies a larger standard deviation at a specific time and location along the sensing fiber, which in turn is indicative of higher vibration intensity experienced by the cable section.

The figure displays the vibration intensity for three distinct types of cables during the experiment conducted on the same day. The study commenced with a control experiment featuring no leakage, followed by the sequential introduction of 1", $\frac{3}{4}$ ", $\frac{1}{2}$ ", and $\frac{1}{4}$ " leakage holes at the bottom of the test pipe. For each hole size, flow rates of 2, 6, 10, 14, and 18 m/s were examined. Figure 9 clearly reveals variations in fiber vibration intensity at different flow rates, with higher flow rates inducing stronger vibrations across all cable types.

Notably, more intense vibrations are visible near the pipe's center, where the leakage was introduced, for both black and flat cables. The vibration anomaly appears to diminish with decreasing hole size and is entirely absent in the control tests.

To quantify the vibration anomalies associated with the leakage points, we calculated the average vibration intensity over a four-minute span in the middle of each experiment. This average intensity forms a vibration profile for each cable, and the amplitude is then converted to decibels (dB) for easier comparison.

Figure 10 showcases the sensitivity of different cables to varying leakage sizes. At a flow rate of 10 m/s, all three cable types can detect a vibration anomaly when the leakage hole is larger than $\frac{1}{2}$ ".

Leakage detection sensitivity is also influenced by the gas flow rate within the pipe. Figure 11 illustrates the vibration distribution along each internal fiber cable at different flow rates. For instance, in the control experiment, vibration intensity escalates with increasing flow rates for the flat cable, and no vibration anomaly is observable at the pipe's center. Conversely, in the experiment with a $\frac{1}{2}$ " leakage hole, a vibration anomaly is observable at all flow rates for both flat and black cables, whereas for the thick cable, the anomaly is only evident at 10 m/s.

Our findings suggest that black and flat cables offer the most reliable leakage detection results to date. Their lighter and more flexible structures likely render them more sensitive to fluid movements within the pipe.

Lastly, it should be noted that we were unable to achieve satisfactory detection results with external cables, likely due to poor mechanical coupling between the cable and the steel pipe.

To better understand the cable vibrations induced by leakage, we conducted a Fourier spectrum analysis on the DAS measurements. The primary objective of this analysis is to identify the frequency range associated with the leakage-related signals. Acquiring this information will aid in optimizing leakage detection algorithms and refining future data acquisition parameters.

In our analysis, raw DAS data were segmented into 10-second intervals, and the amplitude spectrum was computed for each channel. To improve statistical reliability, spectra obtained from 4-minute measurements during the same experiments were stacked and averaged. The resulting spectra are organized as 2D arrays, where each column represents the spectrum amplitude for a specific frequency and each row corresponds to the amplitude spectrum for an individual channel.

Figure 12 illustrates the 2-D spectra obtained from experiments involving various leakage sizes at the bottom of a pipe with a flow rate of 10 m/s. High amplitude spectra are conspicuously evident near the leakage points (indicated by blue arrows in Figure 12) for most cases involving black and flat cables. However, the leakage point is less identifiable in the spectra of thicker cables.

To visualize the amplitude spectrum induced by the leakage more clearly, we extracted the amplitude values corresponding to the leakage location from the 2D spectra and plotted them against frequency. Figure 13 presents the amplitude spectrum for experiments with different leakage sizes, all at a flow rate of 10 m/s. The right column of Figure 13 shows the amplitude ratio between the leakage and control (no leakage) experiments. Our findings indicate that the vibrational anomalies caused by leakage span a broad spectrum. For black cables, we observed up to a 10 dB increase in amplitude across most of the measured frequency range at the leakage point compared to the no-leakage scenario.

The spectral responses appear to be more complex for flat cables. For instance, with leakage sizes of $\frac{1}{4}$ " and $\frac{3}{4}$ ", amplitude increases are more uniformly distributed across the entire frequency band, averaging between 1-2 dB. Conversely, for $\frac{1}{2}$ " and 1" leakage sizes, the amplitude increases are predominantly concentrated in the 1000-2000 Hz range, exceeding an average of 5 dB. This complex response to leakage is likely due to the flow interactions between the flat cable and the flow deviating from the main pipe into the leakage pathway. In contrast, little amplitude increase can be observed on the thick cable, which is consistent with the STD results. At large leakage sizes, amplitude increase can be observed at a narrower frequency band, with 600-800 Hz for the $\frac{3}{4}$ " leakage size and 1100-1300 Hz for 1" leakage size. Further analyses are underway to understand these physical phenomena better.

From the results, we found that the black cable seems to provide more reliable differentiation between leakage and control experiments, which could potentially lead to more reliable leakage detection.

The same analysis was carried out for experiments in which leakage points were introduced at the top and side of the steel pipe. Because these experiments were conducted on different dates from the control experiment, the DAS instrument was disconnected and then re-spliced to the sensing fiber. This action led to a change in the measurement noise floor. Figure 14 presents a comparison of vibration intensity and spectrum analysis for the black cable in both the side and top leakage experiments, conducted at a flow rate of 10 m/s.

We observed that, based on the vibration intensity, spatial identification of the vibration anomaly becomes more challenging for the top and side leakage experiments. Stronger anomalies seem to be associated with smaller leakage sizes, but this trend was not observed at other flow rates or with other cables. The amplitude spectrum results revealed variations in noise levels, which are likely due to the re-splicing of the fiber. Increased amplitude was noted around 1200 Hz for side leakage and 1500 Hz for top leakage. At this stage, it is unclear whether these amplitude increases were induced by the leakage itself.

To improve the reliability of our findings, we plan to redo the top and side experiments, and repeat the control experiment prior to each leakage experiment for more consistent comparison. This approach will help us better identify signal changes specifically attributable to the leakage.

Project Financial Activities Incurred during the Reporting Period:

The following table summarizes the financial activities and the corresponding expenses during the reporting period. Also shown are the budget for the 2nd year and the total expenses in the 2nd year so far. Please note that the actual amount for the expenses might be slightly different from the numbers in the final financial report, since some of the expenses occurring in late of the quarter may not be included in the university’s financial system that we use for managing the funds and expenses by the time the report is submitted. Normally, it takes several days for an expense to be shown in the system after its occurrence.

	Items\Budget and Expenses	Budget for Year 2	Total Expenses in Year 2 So Far	Expenses During Reporting Period
1	Faculty Salaries and Wages including Fringe Benefits	\$28,510	\$28,191	\$7,431
2	Student Salaries	\$65,920	\$58,535	\$18,365
3	Graduate Student Tuition	\$46,260	\$47,364	\$23,848
4	Experimental Expenses (experimental work supplies, services, maintenance, cables, etc.)	\$27,000	\$21,255	\$10,597
5	Travel	\$3,000	\$1,750	\$875
6	Indirect Costs (51.5%)	\$64,703	\$55,997	\$19,193
	Total	\$235,392	\$213,092	\$80,309

Project Activities with Cost Share Partners:

The cost shares are the AY efforts of the PI and co-PIs. Activities are the same as above.

Project Activities with External Partners:

No external partners.

Potential Project Risks:

The risks remain the same as stated in the previous quarterly or annual reports.

Future Project Work:

In the next 30 days, we will:

1. Conduct the multiphase flow experiments for Task#2 at a different liquid flow rate and perform corresponding data processing.
2. Continue experiments for Task#6 as explained in the project activities and perform corresponding data processing.

In the next 60-90 days, we will:

1. Conduct experiments for Tasks#3 and #4 as stated in the project activities and perform corresponding data processing.

Potential Impacts to Pipeline Safety:

Tasks#1 and #2 can potentially help identify and characterize the possible liquid accumulation in a gas gathering or transmission pipeline using DAS, while Tasks#3-6 will potentially help detect the internally corroded surface, deformation, infrastructure damage, and leakage in a gas pipeline.

Appendix

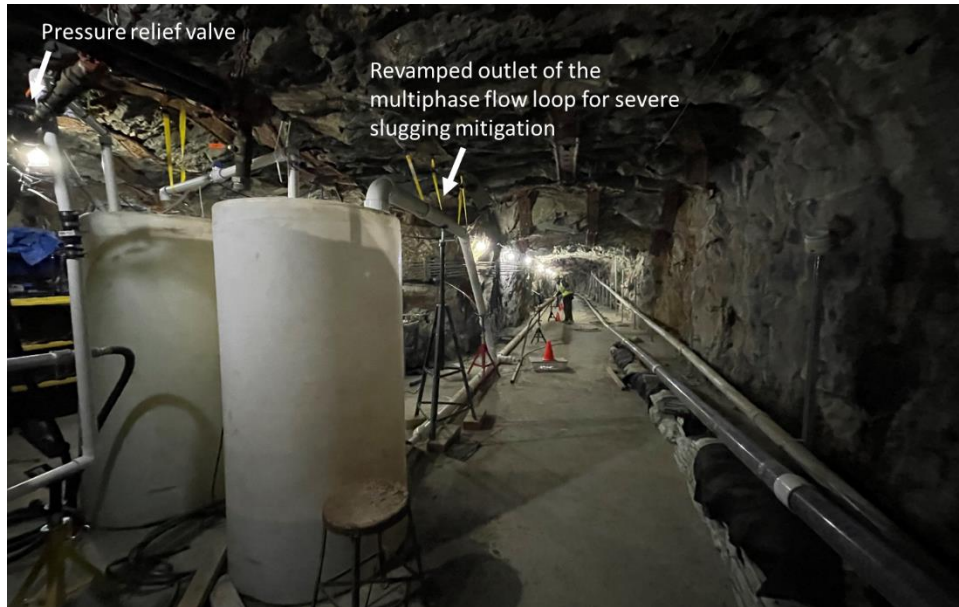


Figure 1. Picture of the multi-phase flow loop

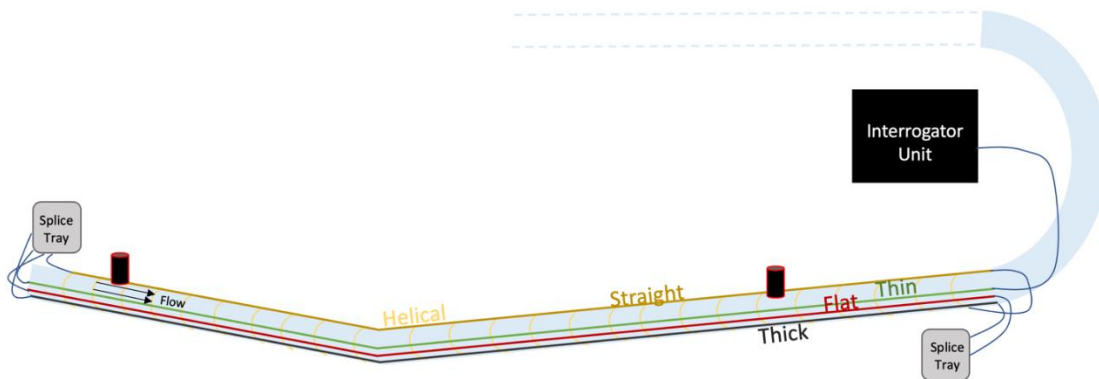


Figure 2. Schematic of Task #2 Layout, depicting the interrogator unit spliced to a sequence of cables - thin, flat, thick, straight, and helical. Two sensors are positioned both uphill and downhill along the experimental section of the flow loop.

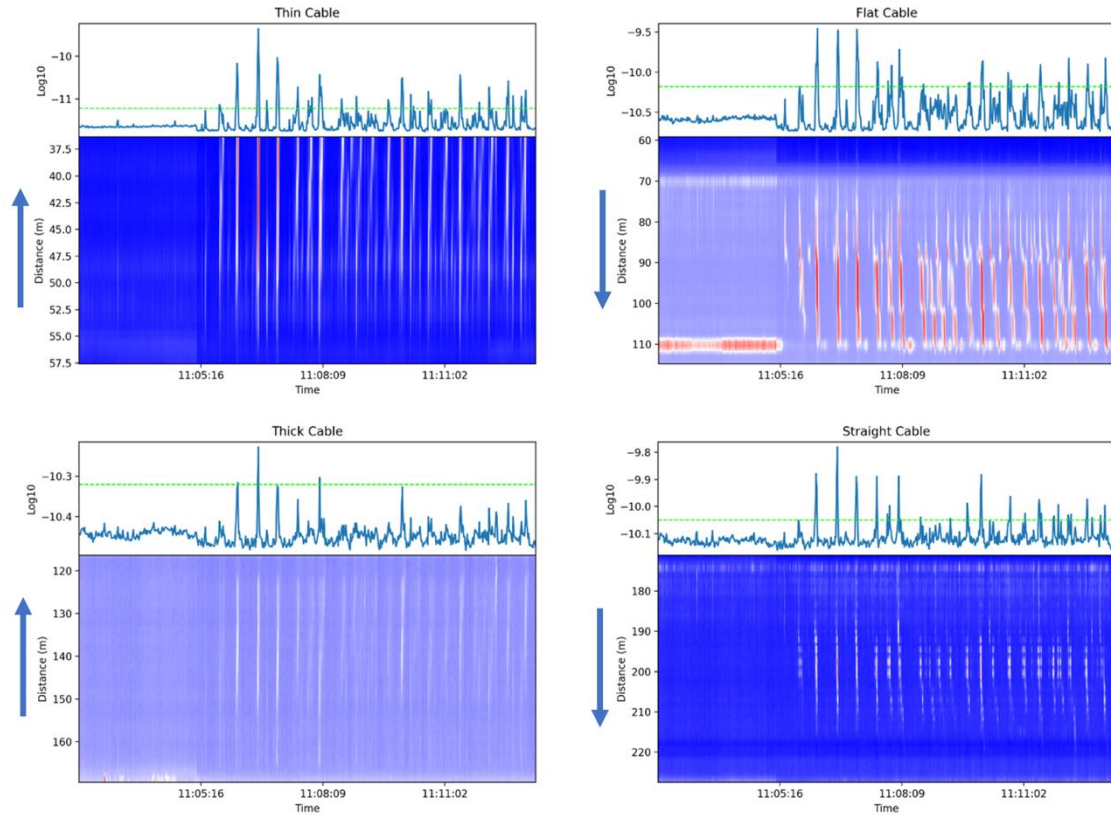


Figure 3. Waterfall plots of processed DAS data, standard deviation DAS data for every second per channel, for the thin, flat, thick, and straight cable designs. Top plots on top of waterfall plots show the average standard deviation of the channels that correspond to the different cable designs. The high standard deviation log-scaled values correspond with slugs observed in the multiphase flow. The air flow velocity changes from 8 to 6 m/s at around 11:05:16. Before this time, the flow is stratified flow without any slugs. After this point, slug flow appears.

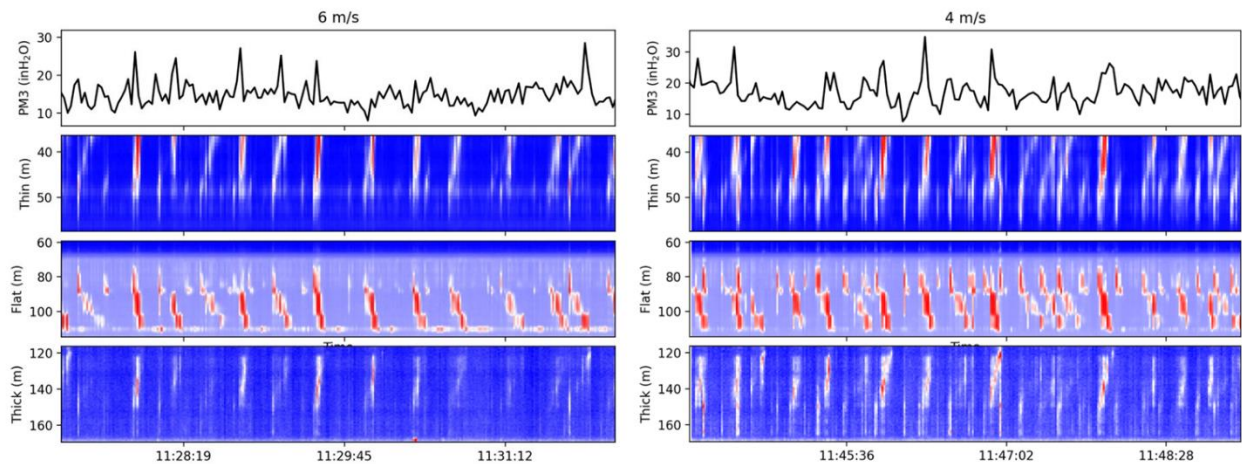


Figure 4. These waterfall plots include the cable sections for the thin, flat, and thick cable designs for different air flow rates (6, 4, and 2 m/s). The top plots are the corresponding pressure measurement in the middle of the uphill section. Overall, the slug signal from DAS corresponds well with that from the pressure measurement.

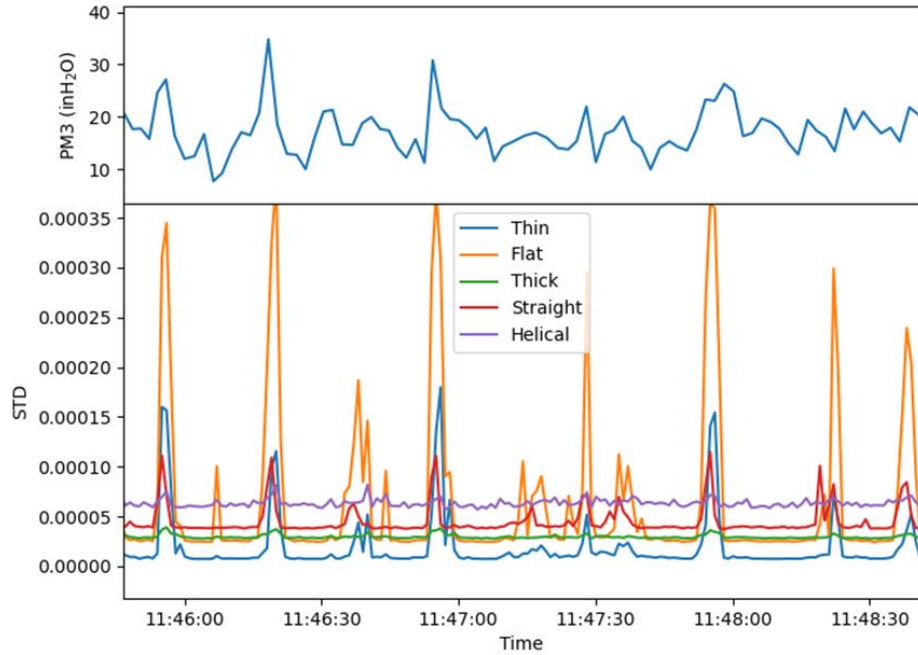


Figure 5. The bottom plot shows the single trace at location near uphill pressure sensor location for each cable design - thin, flat, thick, straight, and helical cables of processed DAS data. The top plot is the corresponding pressure measurement. Here, we can observe that the flat cable has the largest sensitivity to slug detection, followed by the thin, straight, helical, and thick cables.

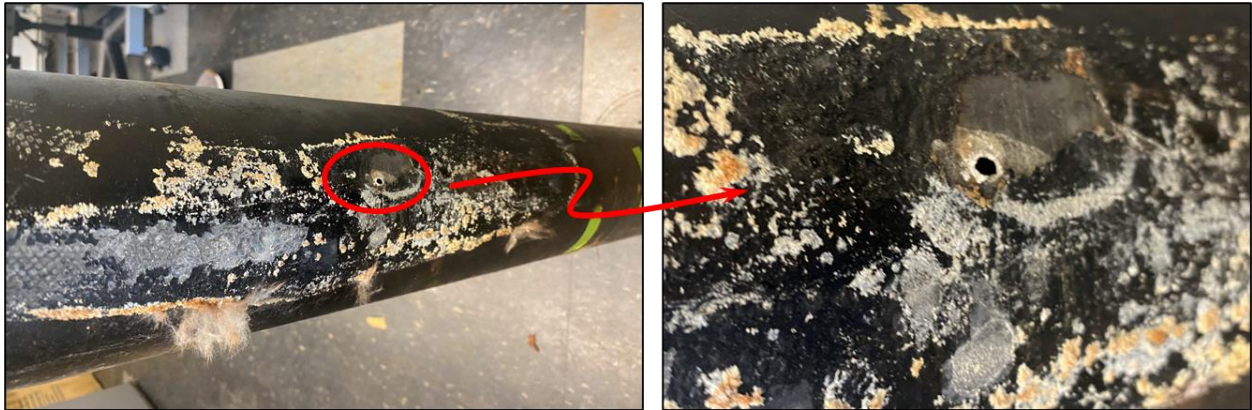


Figure 6. Photograph of the pipe bottom with breakthrough spot



Figure 7. Photograph of the facility that created the dents and the 1-m test sections with two dent sizes.

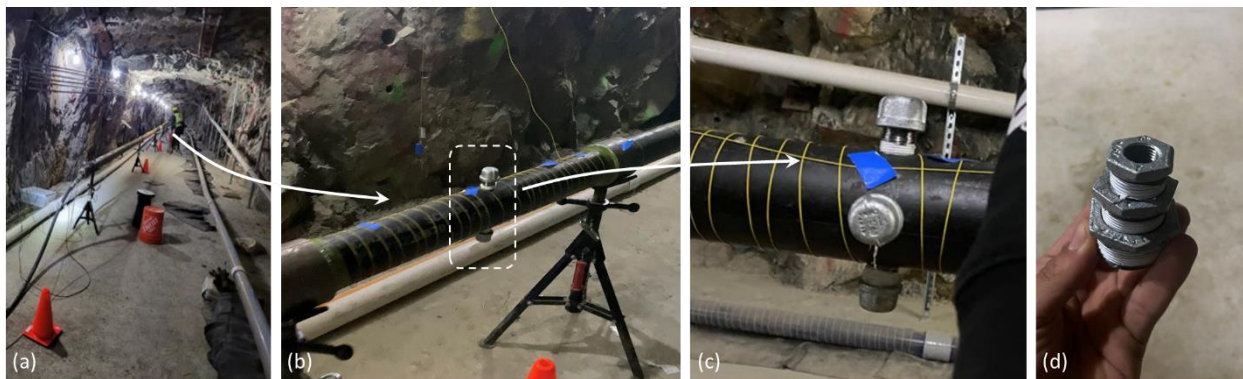


Figure 8. (a) A picture of the facility; (b) 1-m test section for leakage detection; (c) holes with caps on the 1-m test section; (d) reducers for hole size control

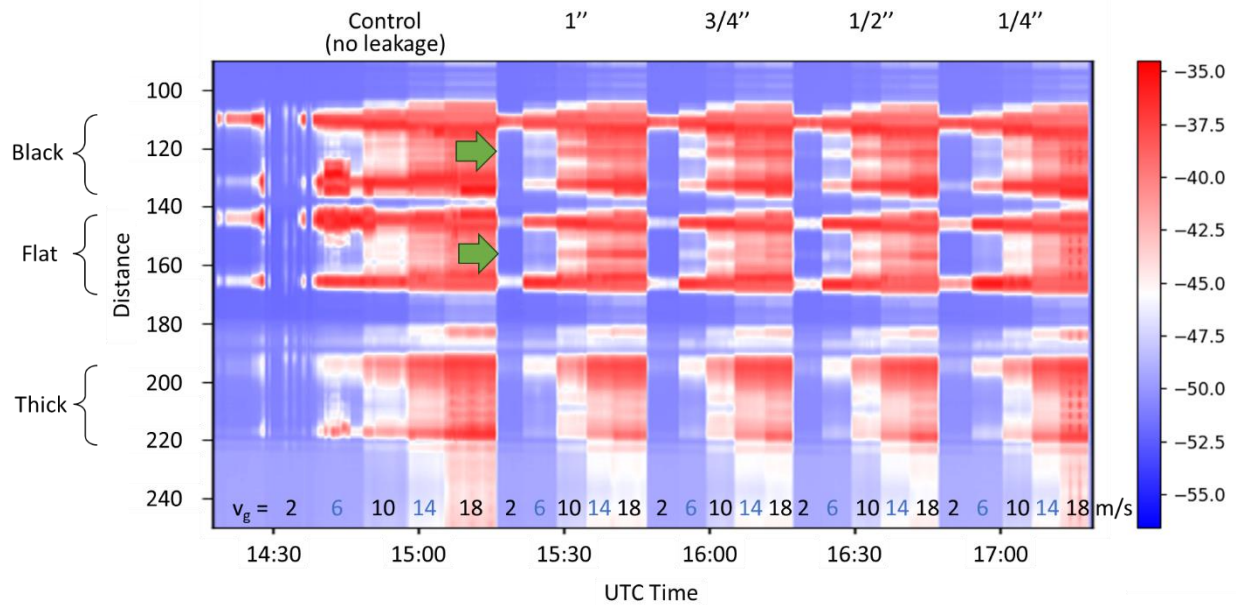


Figure 9: Magnitude of standard deviation values along the fiber during the experiment on August 17th, 2023. For each hole size, the flow rate changes from 2, 6, 10, 14 and 18 m/s. The gas velocities are indicated at the bottom of the image.

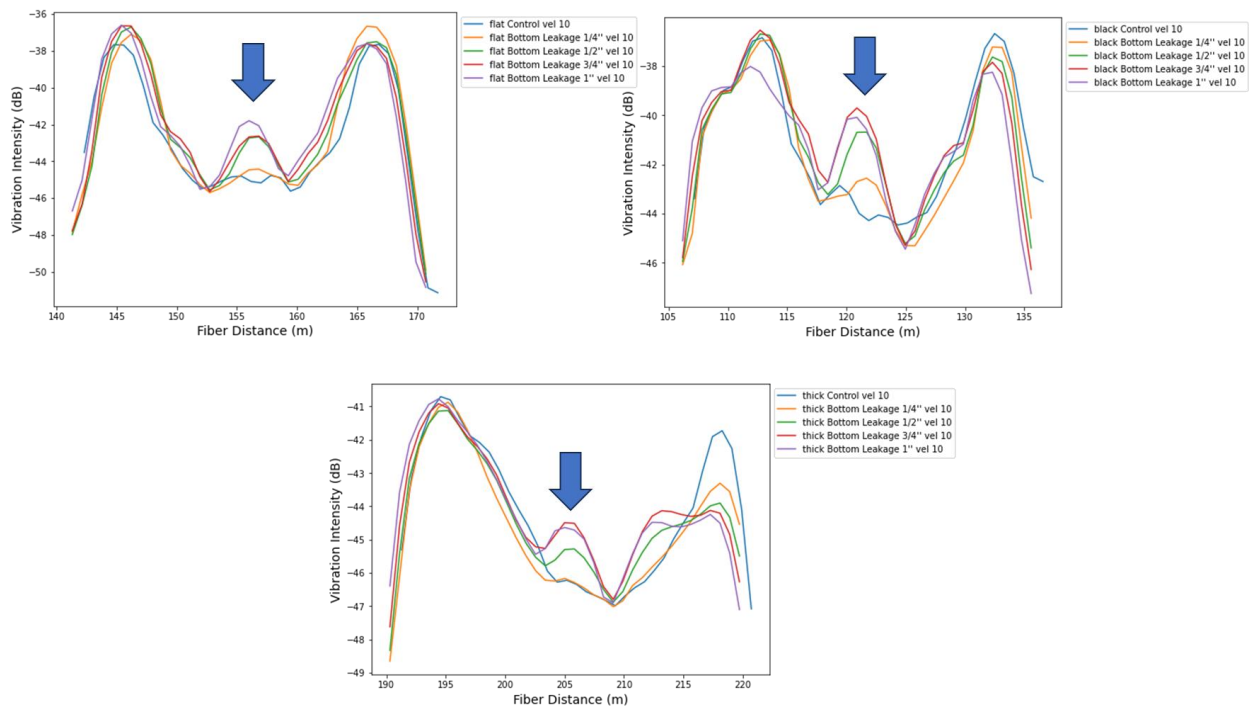


Figure 10: vibration intensity profiles in flat (upper left), black (upper right), and thick (bottom) fiber sections during the leakage experiment. The different curves represent vibration intensities associated with varying leakage hole sizes at a flow rate of 10 m/s. Anomalies in vibration, induced by leakage holes and marked by blue arrows, are observable in all three cable types when the hole size exceeds 1/2 inch.

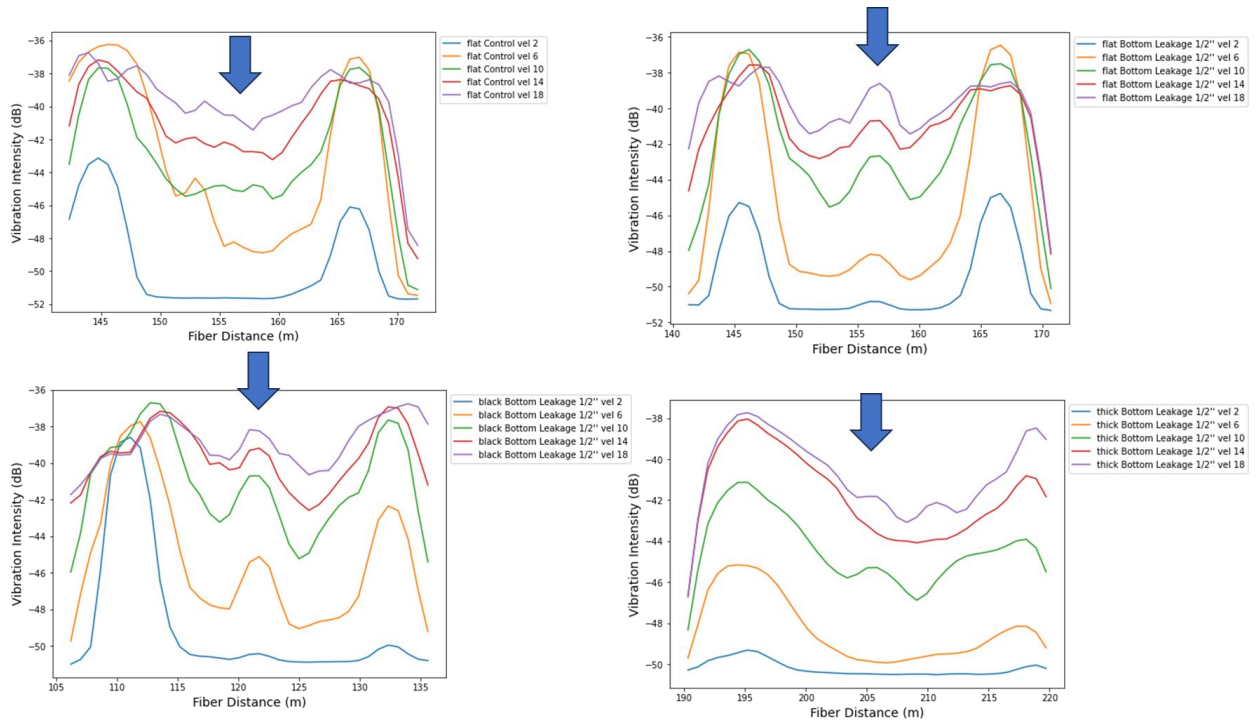


Figure 11: This figure compares the leakage detection sensitivity across different cable types at varying flow velocities. Top left shows a flat cable without leakage as a control experiment. Top right features a flat cable with a leakage hole size of 1/2 inch. The bottom left and bottom right sections present the black cable and thick cable with the same leakage size, respectively.

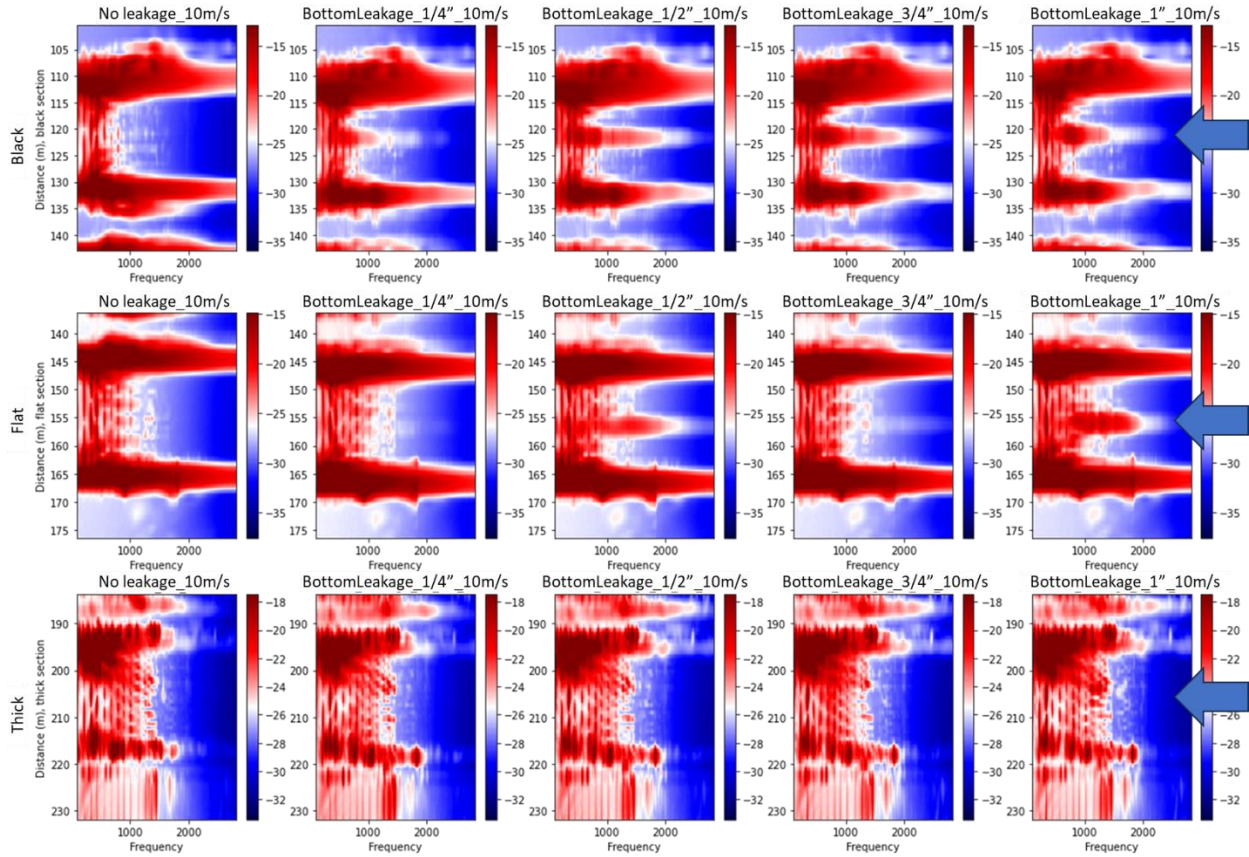


Figure 12: 2D spectra of fiber sections with varying leakage hole sizes at the bottom of the pipe, measured at a flow rate of 10 m/s. The top row displays the black cable section, the middle row showcases the flat cable section, and the bottom row features the thick cable section. Columns from left to right represent the control experiment (no leakage), followed by leakage sizes of 1/4", 1/2", 3/4", and 1", respectively. The color scale is measured in dB. Blue arrows show the leakage point location.

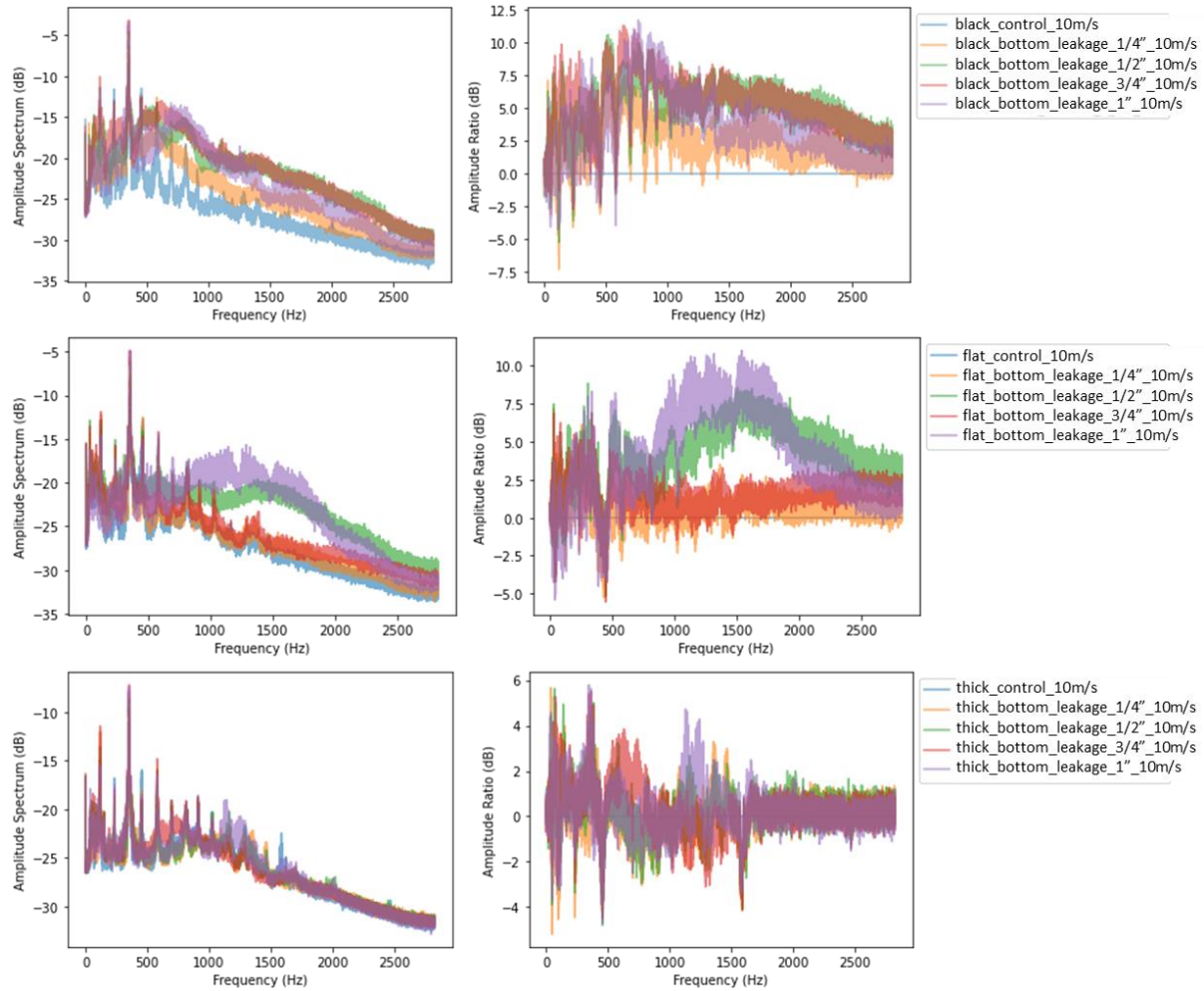


Figure 13: Amplitude spectrum at leakage point locations for various cables and leakage sizes. The flow rate is 10 m/s. The first row displays results for black cables, the second row for flat cables, and the third row for thick cables. The left column shows the amplitude spectrum, while the right column presents the ratio of amplitude spectrum between leakage experiments and the control experiment. All values are expressed in decibels (dB).

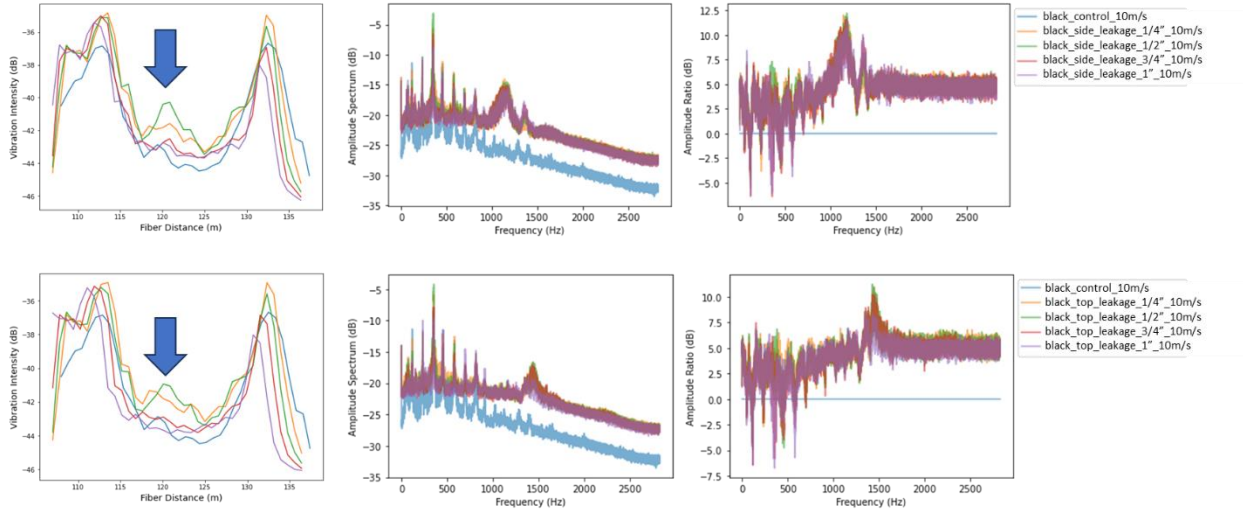


Figure 14: Results from experiments with the black cable where leakage points were introduced at the side and top of the pipe. Top row: side leakage experiments. Bottom row: top leakage experiments. Left column: vibration intensity profiles with varying leakage sizes. Middle column: amplitude spectra at the leakage points. Right column: amplitude ratio between the leakage experiments and the control experiment. The leakage experiments were conducted on different dates than the control experiment, and the fiber was respliced between experiments.